Mechanics and Materials in Design of a Buckling Diaphragm Wave Energy Converter

H. R. Le*[1], K. M. Collins[1], D. M. Greaves[1], N. W. Bellamy[2]

[1]School of Marine Science and Engineering, Plymouth University, United Kingdom
[2]Sea Energy Associates Ltd, Ergo House, Mere Way, Ruddington Fields, NG11 6JS Ruddington, UK

*Corresponding author: *Tel +44- 1752-586172; Email – huirong.le@plymouth.ac.uk*

Abstract

The design of a flexible wave energy device with a spine shape diaphragm proposed by Sea Energy Associates Ltd. was analysed. The operation of the device involves reversible buckling of a diaphragm in both longitudinal and transverse directions. The design constraints of the diaphragm were identified and Cambridge Engineering Selection software was applied to select candidate materials for the diaphragm structure. Best candidates of materials were identified for both laboratory scale and industrial scale. The initial curvature of the diaphragm was analysed using the minimum energy principle. The theoretical predictions of transverse deflection and longitudinal radius of curvature were in good agreement with measurements taken on a 1/10th scale-model of the diaphragm structure.

Keywords: Wave energy converter; material selection; deployable structure; buckling analysis; structural analysis

Nomenclature

- α Factor of end conditions in 3-point bending, 1 for simply supported, 4 for double clamped
- Δ Interval of measurement along the length
- ΔL Longitudinal displacement of spine
- ΔP Contact pressure (or the air pressure it can seal)
- ε_1 Maximum bending strain of diaphragm
- ε_2 Maximum bending strain of spine
- κ Curvature of spine
- e_1 Elastic energy of diaphragm section
- e_2 Elastic energy of spine
- e_t Total elastic energy of the structure
- h Deflection of diaphragm section
- h_1 Transverse deflection of diaphragm edge
- h_2 Transverse deflection of spine
- t_1 Thickness of single diaphragm sheet
- t_2 Thickness of spine
- B_1 Initial width of the diaphragm
- B_2 Width of the spine
- C Deformation constant of structure
- E_1 Elastic modulus of diaphragm
- E_2 Elastic modulus of spine
- I_1 Second moment of bending
- L_0 Initial length of the diaphragm
- R_1 Radius of curvature of diaphragm in transverse direction
- R_2 Radius of curvature of spine in longitudinal direction
- P_1 Load per unit length exerted by the spine onto the centre of the diaphragm
- T Traction in the membrane
- T' In-plane compression in diaphragm per unit length
- V_2 Volume of the spine
- W Width of each diaphragm section

1. Introduction

The need to explore and develop new renewable energy sources is well understood. Globally, we need to reduce our dependence of fossil fuels and to reduce our carbon emissions. The reduction of CO_2 emissions is not only driven by the desire to combat climate change but now forms part of UK legislation. The UK requires approximately 350 TWh/year of electricity, and with up to 840 TWh/year available in UK and Irish waters through wave action (1), meeting a significant proportion of the UK's electricity needs should be technically and economically viable. For the UK, wave and tidal marine renewable energy is seen as having the potential to provide 15 – 20% of current electricity demand within the timeframe of 2050, and is likely to have a similar impact globally (2). The UK holds a leading position (3, 4) in the new wave and tidal industry and it has the potential to become a major export sector for the UK (5).

However, many of the marine energy devices being developed are demonstration or prototype deployments, with only ten full-scale, grid-connected devices deployed by the end of 2011 (3). Unlike in other sectors (marine current, tidal, wind) there is a lack of convergence of technology in the wave energy converter sector that can be ascribed to the different natures of wave resources around the world (6). This diversity in technology means that there are fewer developers trying to solve the same problems than in other industries.

There also remain considerable risks associated with the industry, both from financial and technological points of view (1). Some of the reasons for the slow start to the industry are attributed to high costs of deployment and operating offshore; lack of investment due to the current economic climate; high level of risk and survivability of device and components; long planning and consenting stages and uncertainty of the full cost of energy (1, 2, 7).

The economic viability of each wave energy converter (WEC) is determined by the amount of money that can be made once the capital and operations costs have been taken into account. This is usually expressed as LCOE (levelised cost of energy). The UK's Carbon Trust estimates that by 2050, the LCOE of ocean energy could be 15 pence/kWh. For comparison the LCOE for natural gas is approximately 8 pence/kWh (8, 9). Leijon *et al.* (10) note that the costs of development are driven by the highest energy sea states, the income derived from WECs is related to the commonest sea state.

Wave energy devices show little convergence of technology (1, 2) and it is thought that continued innovation may allow costs to fall faster than for tidal technology, for which there is

more convergence (2). Based on this, the Carbon Trust suggests that there is potential for a step-change in wave energy technology (2). Drew, Plummer and Sahinkaya (11) give a good review of wave energy converter types, noting that there are three broad categories (attenuators, point absorbers and terminators), with numerous operating principles. The European Marine Energy Centre (12) elaborates on the categorisation of the currently available WECs to include nine different types, which can be sorted into three categories: shore-line, bottom-mounted and floating devices. More recently, Babarit *et al.* (13) undertook a numerical study of eight different wave energy device types to benchmark their performance in a variety of sea states.

Bottom-mounted devices such as Aquamarine's Oyster (surge converter) (14) incur high construction, installation and maintenance costs (15) due to the requirement for seabed anchoring and inefficient pumping systems. A principal advantage of pumping a working fluid, as with the Oyster, is that the power take-off mechanism can be separated and even placed onshore to reduce some of the maintenance costs. Semi-submerged attenuators such as Pelamis have advantages in ease of maintenance, since they can be towed to calmer waters to be repaired, but they may still incur high construction costs. Shore line devices, such as breakwater-mounted oscillating water columns present the cheapest option for maintenance and can be very robust but their response can be narrow banded if not actively controlled. Semi flexible floating bags containing compressed air to drive a turbine are called 'clams' (16). These devices have low construction costs but are always mounted on some supporting structure. The all-fabric conical free-floating clam (17) uses a new principle that it shrinks as it sinks. This lengthens the resonance period, so that it can be tuned to long waves. The efficiency is yet to be proved.

Sea Energy Associates Ltd. (SEA Ltd.) is a device developer hoping to progress its design to the point of scale sea trials. Its device – the SeaWave – has been designed to obtain a more favourable cost of power. The SeaWave is intended to combine the advantage of semi-submerged attenuators, the separation of capture device and power take-off (PTO), as in the surge converters, and the low materials costs of the clam-type devices. By being a semi-submerged device, installation and maintenance costs should be lower than for a bottom-mounted device and its operating principle, which is a combination of attenuator and pump, relies on the wave celerity (phase velocity), which is faster than wave orbital velocity.

It is noted that the design and material selection are vital to the survivability and durability of all WECs (18, 19). To select the desirable materials requires full understanding of the

mechanism, the design constraints and the operation environment. Therefore an introduction to the structure is provided in the following section.

2. SeaWave device

The SeaWave wave energy converter consists of a long flexible hose with a central diaphragm (20). The structure takes the form of the skeleton of reptiles but it curves by stretching the spine instead of contracting the hose. It is a type of deployable structure. The diaphragm at the centre of the hose is pre-stressed by a central spine so that it buckles and forms a wave shape. The stiffness of the structure is tailored so that it can be coupled with a water wave, Figure 1. By coupling to the surface, the crest of the diaphragm will be displaced along the device at the wave celerity. This motion of the diaphragm crests will move pockets of air along the hose to the end section where compression can occur by controlling the output flow rate. The pressurised air can then be used to run an air turbine to generate electricity. Compared to many other devices, this is a lightweight semi-submerged structure which will reduce deployment and maintenance costs. It has the potential to improve energy conversion efficiency due to the ability to adapt to the frequencies of the wave. The energy output relies on the volume of compressed air generated rather than the pressure. That means a thinner diaphragm and hose can be used so that less expensive materials can be used. Therefore the manufacturing cost of the device is expected to be cheaper than other wave energy devices.

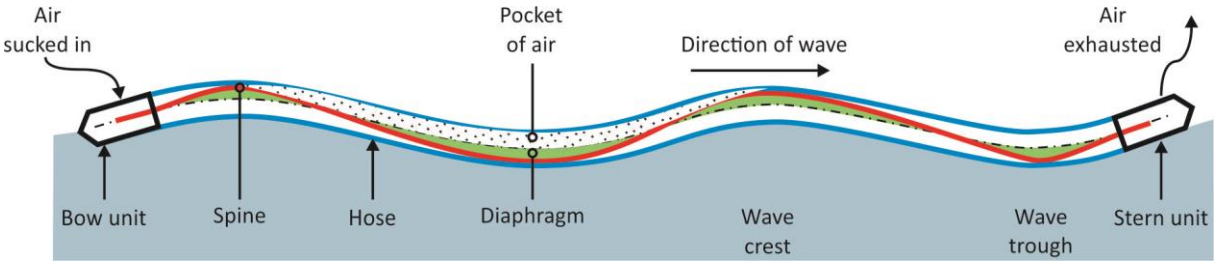

Figure 1 - The buckled SeaWave device will couple to the surface of the wave.

The diaphragm will determine the performance and the service life of the structure in a large part. The basic structure of the diaphragm is made up of a series of diaphragm sections linked by a longitudinal spine at the centre and two strings or stiffeners on the edges to restrain the extension of the edges. When the central spine is pushed in, the diaphragm sections will bend in transverse while the spine buckles into a waveform. Several models have been developed using various materials and designs by trial and error. A 1/10th laboratory scale model produced using plastics for both the diaphragm and spine with a PVC

hose has been tested in the wave tank. Fracture of the spine has been a problem because it is a long structure. Another issue identified is the sealing between the diaphragm and the hose. To prevent air from flowing backward, a seal between the crest of the spine and the hose is required. The energy capture efficiency is directly proportional to the output air pressure achieved. Therefore sufficient in-plane stiffness is required of the diaphragm. On the other hand, this will increase the longitudinal bending stiffness of the device and hinder the coupling with the wave. A systematic analysis of the structure is needed to resolve the contradiction and to optimise the design before the device can be operated successfully.

During operation, the buckling of the diaphragm is reversed under the action of waves so that the bending of both the diaphragm and the spine is reversed. Therefore the structure is subjected to completely reversed stress. At WaveHub (a grid-connected facility in the UK where sea-trials can be undertaken), the most likely wave has a period of ~5.5 s and a height of ~1.5 m (21). This translates to a wavelength of around 47 m travelling at 8.6 m/s. If this were the only wave encountered by the device, it could expect to see more than 5 million cycles per year. Therefore fatigue failure will be a major limiting factor of the spine and the diaphragm sections for long-term operation. This is worsened by the corrosive marine environment which will reduce the fatigue strength of most materials significantly in particular the metals. These factors must be considered in the design and material selection.

This paper is aimed to identify the main constraints in the design of the diaphragm and general guidelines in material selection. The mechanics of the spine buckling mechanism will also be analysed for the manipulation of the initial shape of the diaphragm. The theoretical predictions of the deflection and the longitudinal radius of curvature will be validated by the measurements taken on a small scale plastic model.

3. Design of the diaphragm

Figure 2(a) shows the construction of the diaphragm of a 1/10th model comprised of a thick polycarbonate plastic spine in the centre and thin polyethylene terephthalate **(**PET) plastic sheets as the diaphragm with a screw control mechanism at one end. The PET sheets are split into sections with a gap of about 5mm and joined along the edges. The connection of each diaphragm section and the spine is illustrated by Figure 2(b) showing the central spine, the diaphragm sheets and the hinge mechanism at the edges. The diaphragm itself is made of two layers pulled together at mid-width with plastic rings which allow the central spine to slide along the length. The edges of the two diaphragm layers are both hinged to a side string so that the diaphragm section is free to rotate. The advantage of this modular design

concept is that it allows for repair of each section in service if needed and it can be augmented along the length for ease of transport and deployment.

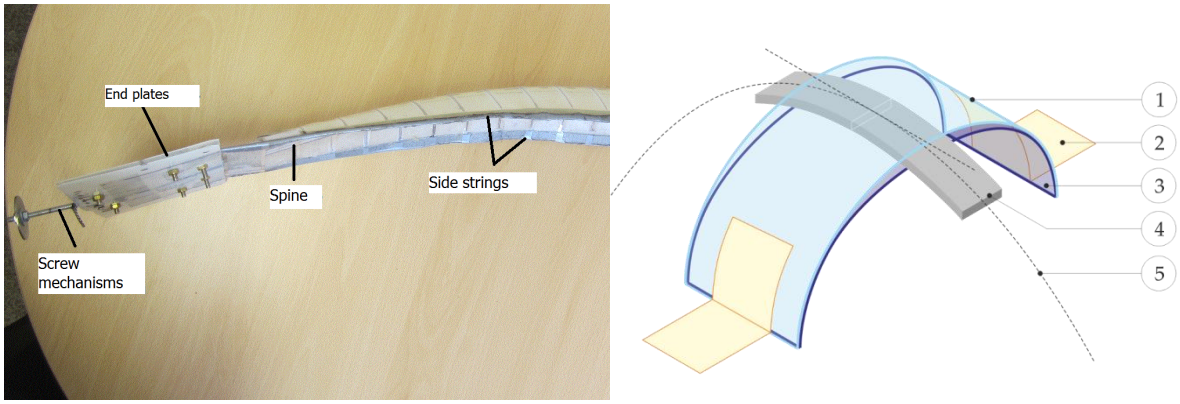

(a) (b)

Figure 2 – (a) 1/10th scale diaphragm model, (b) cross section of the diaphragm: 1 – diaphragm top sheet; 2 – hinge; 3 – diaphragm bottom sheet; 4 - spine; 5 - central line

Bending strain constraint

When the spine buckles under compression from the screw mechanism, the diaphragm sections also bend in the transverse direction. Since the ends and edges of the diaphragm section are free to rotate, each sheet can be modelled as a single sheet under 3-point bending. Assuming a circular arc of cross-section, as shown in Figure 3, the maximum bending strain in the diaphragm section can be derived using classic bending mechanics (22, page 126):

$$\varepsilon_1 = t_1/R_1 \qquad (1)$$

Where: ε_1 – maximum bending strain of the diaphragm, t_1 - the thickness of the diaphragm, R_1 - the radius of curvature of the diaphragm.

As a typical example of a 1/10th scale model, t_1 = 0.5 mm, R_1 = 50 mm, the maximum bending strain will be ε_1 = 1%. This large strain will impose a constraint on the materials available. Most metals, which have a typical yield strain of ~0.3% are ruled out, leaving plastics, which have a typical failure strain of 1 – 2% and carbon fibre reinforced plastic (CFRP) of 0.5 – 1% [5]. Therefore only plastics and advanced composites can stand such high level of strain in corrosive marine environment.

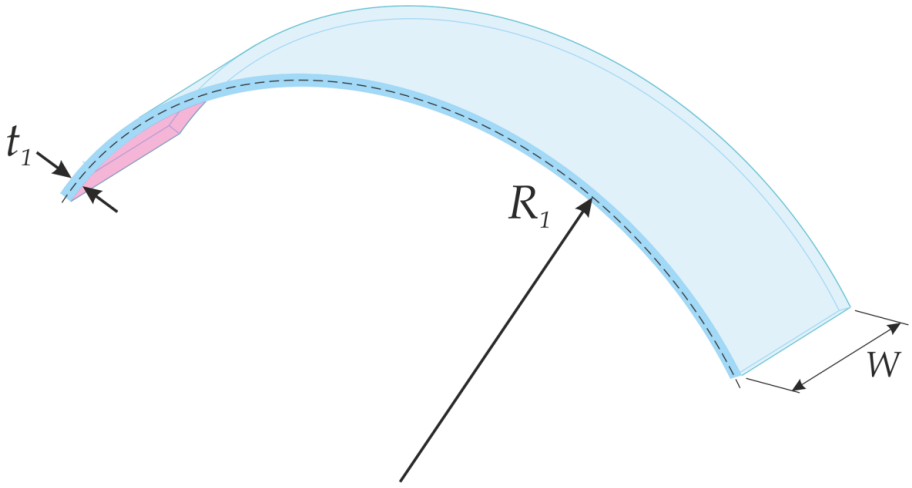

Figure 3 - Bending strain in diaphragm sections

Buckling of diaphragm sections

To avoid back flow of air between two layers of material in contact will require sufficient contact pressure between them. As shown in Figure 4, stretching a layer of rubber on a diaphragm section will generate a contact pressure between the rubber and the diaphragm. Applying the membrane solution to the hose (22, page 150) gives:

$$\Delta P = \frac{T}{R_1} \qquad \textbf{(2)}$$

Where: ΔP - the contact pressure (which is the maximum air pressure it can seal), T - the traction in the rubber or compression in the diaphragm, and R_1 - the radius of curvature of the diaphragm. For a constant tension in the rubber, the maximum contact pressure occurs at the crest of the spine where R_1 is at a minimum.

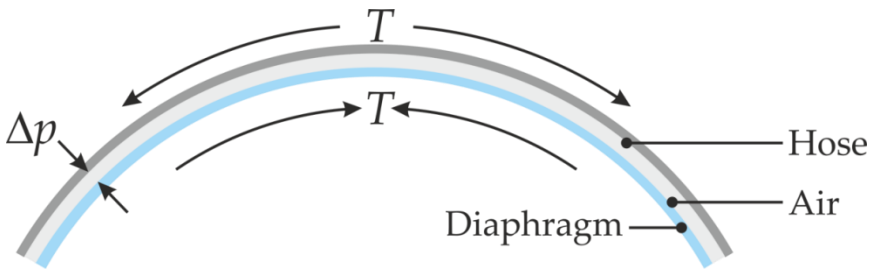

Figure 4 - Contact pressure on diaphragm sections

Therefore to maximise the air pressure is to maximise the allowable in-plane compression applied to the diaphragm sections. The maximum compression applied to the thin diaphragm section is limited by the buckling load limit. The 2nd mode of buckling must be avoided to ensure the diaphragm section remains an arc while an in-plane compression is applied.

The critical buckling load in 2nd mode subjected to end load on 2 parallel sheets (shown in Figure 5) is given by (22, page 219):

$$T = \frac{4\pi^2 E_1 I_1}{(B_1/2)^2} \quad \textbf{(3)}$$

Where: B_1 – the width of the diaphragm, E_1 - elastic modulus of diaphragm, I_1 - second moment of bending for two parallel sheets of thickness t_1 is given by $I_1 = 2 * \frac{W{t_1}^3}{12}$ in which W is the length of each diaphragm section as indicated in Fig. 5.

The critical buckling load for a unit length of diaphragm is hence given by:

$$T' = \frac{8\pi^2 E_1 t_1^3}{3B_1^2} \quad \textbf{(4)}$$

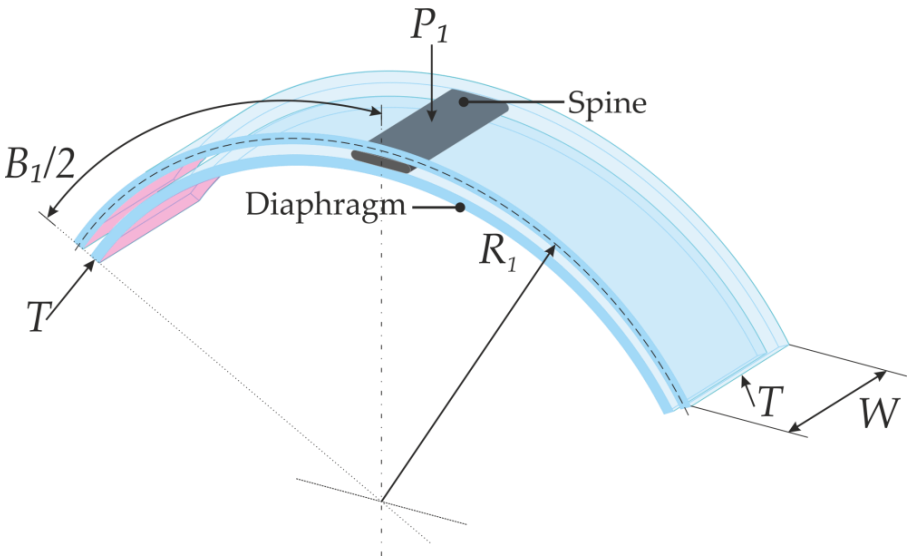

Figure 5 - Buckling of diaphragm sections

4. Material selection for the diaphragm

The objective in the design of this structure is to maximise the transverse buckling resistance, which will require thicker plates, while maintaining deflection or to maximise the cross-section area of hose, which will require thinner plates. Maximum bending stress of diaphragm sections is related to the central load P_1 applied to the material (22, page 127):

$$\sigma_f = \frac{Mc}{I_1} = \frac{3P_1 B_1}{2W \times t_1^2} \quad \textbf{(5)}$$

Where M is the bending moment at the centre, c is the half thickness, P_1 is the force applied to the centre of the section; W – the length of the section.

Assuming a linear force-deflection relationship for a first approximation, the central deflection of diaphragm section due to bending can be approximated by the following formula (22, page 971):

$$h = \frac{P_1 {B_1}^3}{48\alpha E_1 I_1} = \frac{P_1 {B_1}^3}{8\alpha E_1 W {t_1}^3} \qquad \textbf{(6)}$$

Where: α - the parameter for edge condition, which is 1 for simply supported and 4 for double clamped edges.

Eliminating P_1 from Eqs. 5 and 6 gives:

$$t_1 = \frac{\sigma_f {B_1}^2}{12\alpha E_1 h} \qquad \textbf{(7)}$$

Combining Eqs. (4 and 7 to eliminate t_1 gives:

$$T' = \frac{\pi^2 {B_1}^4}{648(\alpha h)^3}\left(\frac{{\sigma_f}^{3/2}}{E_1}\right)^2 \qquad \textbf{(8)}$$

To maximise the buckling limit and hence the air sealing pressure between the hose and the diaphragm is to maximise *T′*, or to maximise the material index, *M*, given by:

$$M = \left(\frac{{\sigma_f}^{3/2}}{E_1}\right) \qquad \textbf{(9)}$$

The Cambridge Engineering Selection Software – CES.2014 is applied to create material's map shown in Figure 6. The material's map is generated using elastic modulus as vertical axis and elastic limit as horizontal axis including six categories of materials: foams, ceramics, natural materials, polymers, composites, metals and alloys. Each shaded area represents one category of materials. Each filled bubble represents the range of properties of one type of material. A selection line based on material index *M* is placed as lowest as possible leaving a limited number of materials underneath the line. The materials below the selection line have highest *M* and thus desirable for the application (23). The best candidate materials based on this criterion are superalloys and CFRPs. The selection line is also touching one natural material – bamboos and titanium alloys. The hardened plastics (PVC, PC, and PET) are immediately behind the selection criterion. Superalloys and titanium alloys can be used for smaller components such as marine turbines (24) but can be ruled out due to their high cost for such a large structure. Bamboos stand out due to their high strength over modulus. However, the properties of these natural materials are subjected to large variability. They also have high water absorption rate which has significant impact on their properties. Therefore the remaining candidate materials are plastics and FRPs which are further discussed below.

Hardened plastics such as polyethylene terephthalate (PET), polyvinylchloride (PVC) and polycarbonate (PC) have the highest allowable strain compared to other candidates and high strength over modulus (23). However, their service life is subjected to creep, corrosion and wear in marine environments. Therefore hardened plastics are satisfactory as materials for laboratory demonstration but they are not desirable for commercial structures.

Advanced fibre reinforced plastic composites (FRP) are recognised as a better choice for marine structures because of their light weight and their high corrosion resistance and fatigue strength (25-28). FRP composites also stand out on account of their high strength over elastic modulus. In particular, CFRP has superior fatigue resistance. The fatigue strength is about 40-50% of the static strength in marine environment compared to 20% of steels (29). Therefore a lighter structure can be made for the same loading conditions. This will reduce deployment costs and maintenance costs due to better corrosion resistance. Therefore the total operation costs over the entire service life of the structure may be lower using CFRPs.

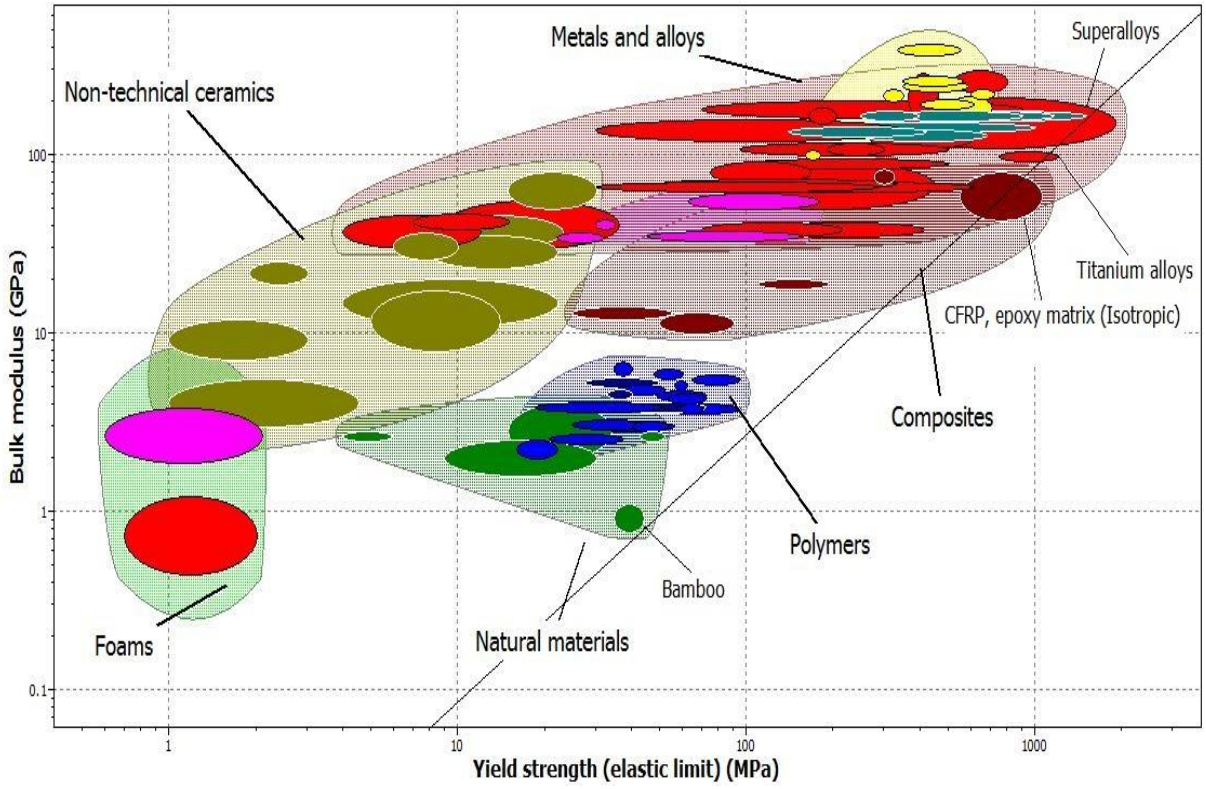

Figure 6 - Material selection map for diaphragm sections using Cambridge Engineering Selection system

5. Manipulation of longitudinal and transverse curvature

As shown in Figure 7, the curvature in both directions will increase while the spine is compressed into the diaphragm. Assuming the spine is an arc and the edge strings are inextensible, the transverse deflection *h* is related to the compression of the spine from geometry:

$$\frac{h}{R_2} = \frac{\Delta L}{L_0} \quad \textbf{(10)}$$

Where ΔL is the displacement, L_0 is the initial length of the spine.

Assuming a linear relationship between central force and deflection, the stored elastic strain energy of all diaphragm sections with a total length L_0 is given by:

$$e_1 = \frac{1}{2}\frac{P_1 h L_0}{W} \quad \textbf{(11)}$$

Solving for P_1 from Eq. (6) and inserting into Eq. 11 gives:

$$e_1 = \frac{4\alpha E_1 {t_1}^3 h^2 L_0}{{B_1}^3} \quad \textbf{(12)}$$

Stored elastic energy of the spine can be derived by assuming an arc with a radius of curvature of R_2:

$$e_2 = \frac{V_2 E_2 {\epsilon_2}^2}{6} = \frac{B_2 L_0 E_2 {t_2}^3}{6{R_2}^2} \quad \textbf{(13)}$$

Where: V_2 – the volume of the spine, E_2 – elastic modulus of spine, t_2 – thickness of spine, R_2 – radius of curvature of spine.

The total stored energy of the structure is the sum of the diaphragm and the spine:

$$e_t = e_1 + e_2 \quad \textbf{(14)}$$

For a static structure with no external force, the potential energy must be at minimum (30, pages 153 - 154). So for any virtual perturbation to the structure, such as an infinitesimal change to the deflection *h*:

$$\frac{de_t}{dh} = \frac{de_1}{dh} + \frac{de_2}{dh} = 0 \quad \textbf{(15)}$$

Then from Eq. 12:

$$\frac{de_1}{dh} = \frac{8\alpha E_1 {t_1}^3 h L_0}{{B_1}^3} \quad \textbf{(16)}$$

And from Eq.13,

$$\frac{de_2}{dR_2} = -\frac{B_2 L_0 E_2 {t_2}^3}{3{R_2}^3} \quad \textbf{(17)}$$

Finally, differentiating Eq. (10) with respect to *h* gives:

$$\frac{dh}{dR_2} = \frac{\Delta L}{L_0} = \frac{h}{R_2} \quad \textbf{(18)}$$

Therefore:

$$\frac{de_2}{dh} = \frac{de_2}{dR_2} \times \frac{dR_2}{dh} = -\frac{B_2 L_0 E_2 {t_2}^3}{3{R_2}^3} \times \frac{R_2}{h} \quad \textbf{(19)}$$

Combining Eqs. 15, 16 and 19 and simplifying gives:

$${R_2}^2 = \frac{E_2 B_2 {t_2}^3 {B_1}^3}{24\alpha E_1 {t_1}^3 h^2} \quad \textbf{(20)}$$

This can be rewritten as:

$$hR_2 = \sqrt{\frac{E_2 B_2 {t_2}^3 {B_1}^3}{24\alpha E_1 {t_1}^3}} = C \quad \textbf{(21)}$$

Therefore *h* and R_2 can be derived by combining Eqs. 10 and 21 so that:

$$h = \sqrt{C\frac{\Delta L}{L_0}} \quad \textbf{(22)}$$

$$R_2 = \sqrt{C\frac{L_0}{\Delta L}} \quad \textbf{(23)}$$

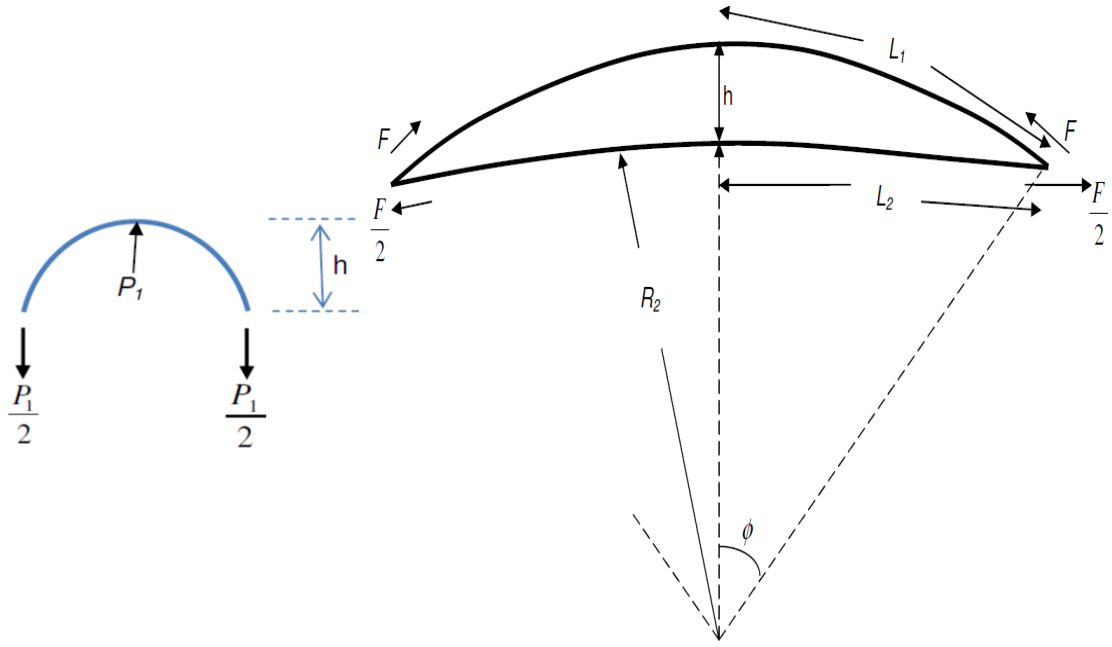

Figure 7 - Deflection of spine and diaphragm sections

To demonstrate the effect that the diaphragm to spine thickness ratio has on the bending, it is useful to consider some example values. Table 1 gives the material properties applied in the analysis of the 1/10th plastic model according to Plastics International (31) and the dimensions measured from the physical model. The effect of t_1/t_2 on hR_2 predicted by the model for the plastic spine/diaphragm is shown in Figure 8.

Table 1 - Material properties of plastic-plastic model.

Component	Material	Elastic modulus, E (GPa)	Width (m)
Diaphragm	PET	3.2	0.125
Spine core	PC	2.3	0.030

The results show that the product of hR_2 decreases with t_1/t_2 as expected considering Eq. 21. Physically, this is because the bending stiffness of the diaphragm increases with t_1 under the same force asserted by the spine so that the transverse deflection h decreases. Given this relationship, it is then possible to select the material combinations and/or geometry in order to provoke a certain bend on the device. It is noted in Fig. 8 that hR_2 decreases with increasing α. When α=1, it represents simply supported edge conditions for the diaphragm sections (c.f. Fig. 7) which means the edge force component in horizontal is zero. The other extreme is when α=4 representing a clamped edge. In reality, the edge condition lies

somewhere between clamped and simply supported. It is movable but there is a horizontal restraining force due to the inward bending. Therefore α should be between 1 and 4.

The property hR_2 can be seen as an indication of the physical device's maximum flow rate and so from an operational point of view, it is a quantity that should be maximised. By increasing h, the difference between the top of the spine and the edge string (7), the internal volume is increased, hence a larger volume of air will be moved along the device per cycle. R_2 is a measure of the longitudinal deflection of the spine and the greater the radius of curvature, the more likely the device will be to couple itself to longer wave lengths (and higher waves). Since the celerity of a water wave is directly proportional to its wave length, an increase in R_2 will lead to faster air pumping rates. The adjustment of h or R_2 can be achieved by varying the spine compression rate as indicated by Eqs. (22) and (23). Whether the better strategy is to maximise h or R_2 depends on the physical properties of not only the device but also the surrounding wave climate.

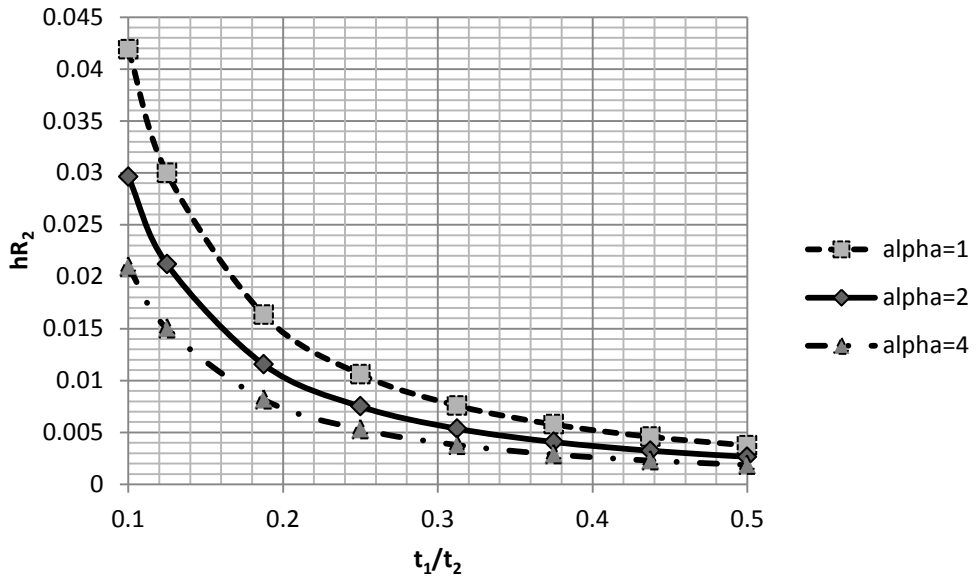

Figure 8 **- Effect of diaphragm/spine thickness ratio on deflection of diaphragm, α = 1-4**

6. Experimental verification of spine control

The 1/10th scale model of the spine and diaphragm was provided by SEA Ltd. for verification of the theoretical model. The model comprised of a plastic (PC) spine of rectangular cross-section 4.3 mm x 30 mm and a series of plastic (PET) diaphragm sections. Each section was made up of two sheets of 0.5mm hinged to a string at the edges. At one end, the strings, the diaphragm and the spine were bolted to two ABS plates of 1 mm thick (Figure 9). At the

other end, the strings and the diaphragm were bolted to the plastic plate while the spine end was in contact with a bolt mechanism. Therefore, the strings were under tension while the spine was compressed. The experimental setup for the measurement of the deflection and the radius of curvature of the spine is shown in Figure 9. To reduce the effect of weight on the deformation, the diaphragm was laid on its side on a smooth flat surface. To ensure the diaphragm was vertical, the two edges were held gently on to a vertical ruler using a soft rubber band. The spine was pushed in by rotating a screw with a standard M4 thread with a pitch of 0.7 mm. The longitudinal displacement of the spine was varied in the range of 1 – 20 mm giving a compression rate up to 2%.

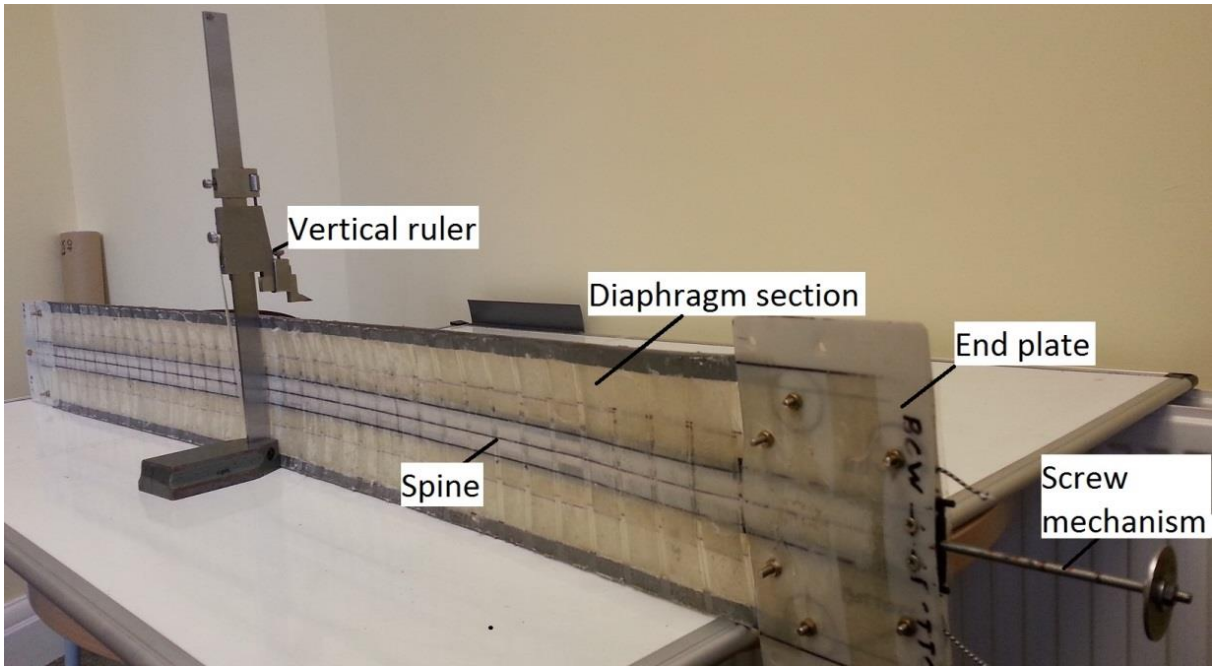

Figure 9 - Experimental set-up for measurement of deflection and curvature

The transverse displacement of the spine h_2 and the edge h_1 were measured using a ruler at five positions of equal intervals of 100 mm in the middle section as shown in Figure 10.

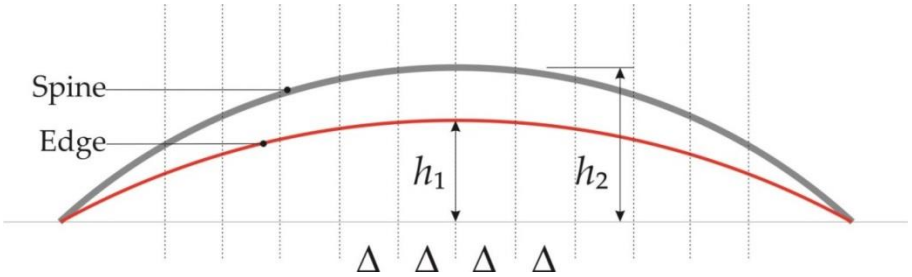

Figure 10 - Schematic of measurement of transverse displacement and curvature

The difference in deflection between the spine and the edge, $h = h_2 - h_1$, was measured using a vernier near the mid-length of the diaphragm and repeated 3 times to obtain mean values reported here.

The spine displacement, h_2, was fitted to a parabolic function using the least square method implemented in MATLAB:

$$h_2 = ax^2 + bx + c \qquad \textbf{(24)}$$

The curvature is derived by the double differentiation of the transverse displacement h_2:

$$\kappa = h_2'' = 2a \qquad \textbf{(25)}$$

where κ is the curvature of the spine in the middle of the section and the radius of curvature, R, is given by the inverse of the curvature, κ.

Figure 11 plots the product hR_2 against the compression rate. The results are in agreement with the theoretical prediction for $t_1/t_2 = 0.125$ given by Eq. (21). However there is discrepancy at low compression rate due to the measurement error and at high compression rate due to some stiffening of the structure with increasing deflection of the diaphragm and spine.

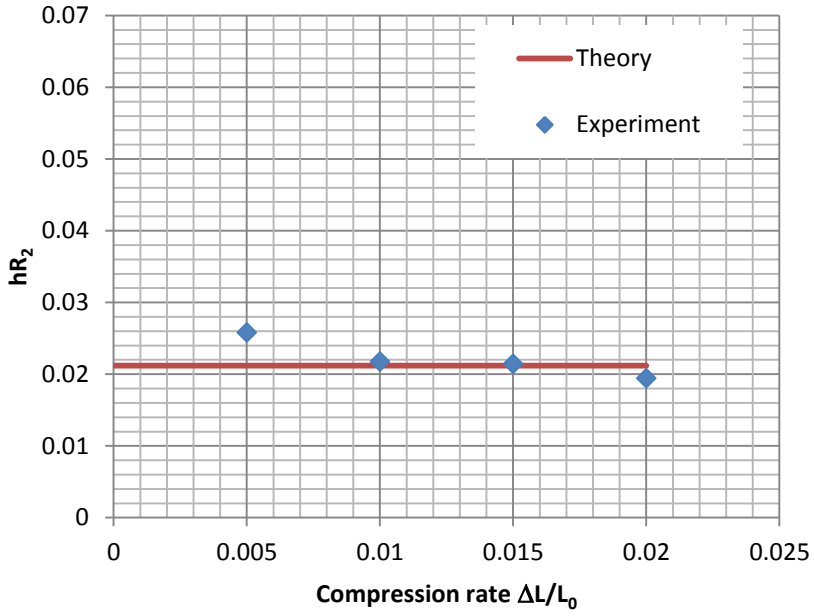

Figure 11 - Comparison of theoretical predictions and physical measurement of hR_2

The transverse deflection h near mid-length is plotted against spine compression rate as shown in Figure 12. It follows the parabolic trend as predicted by Eq. (22). The

measurements are in good agreement with theoretical predictions for $\alpha = 2$, which describes the edge constraint of the diaphragm as between simply supported and double clamped.

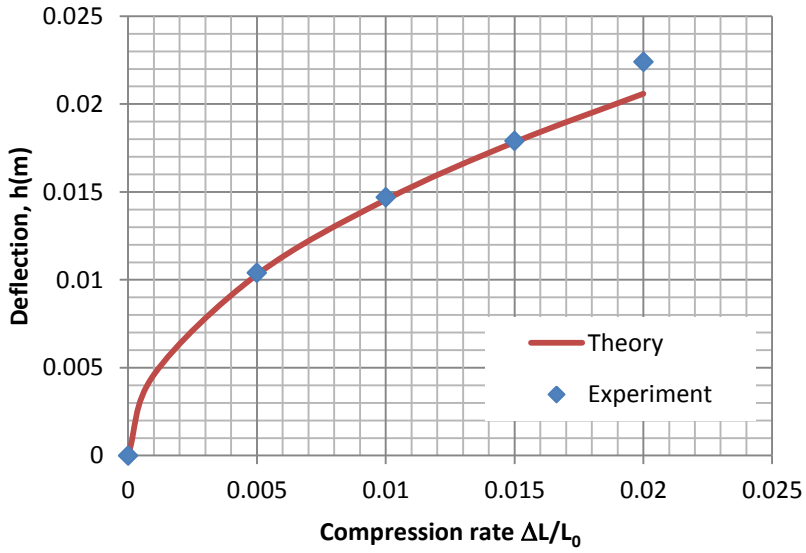

Figure 12 - Transverse deflection of diaphragm

The radius of curvature of the spine is shown in Figure 13 showing good agreement with theoretical prediction by Eq. 23 for $\alpha = 2$. The radius of curvature measured is slightly lower than the theoretical prediction when the compression rate is above 1% owing to stiffening of the diaphragm.

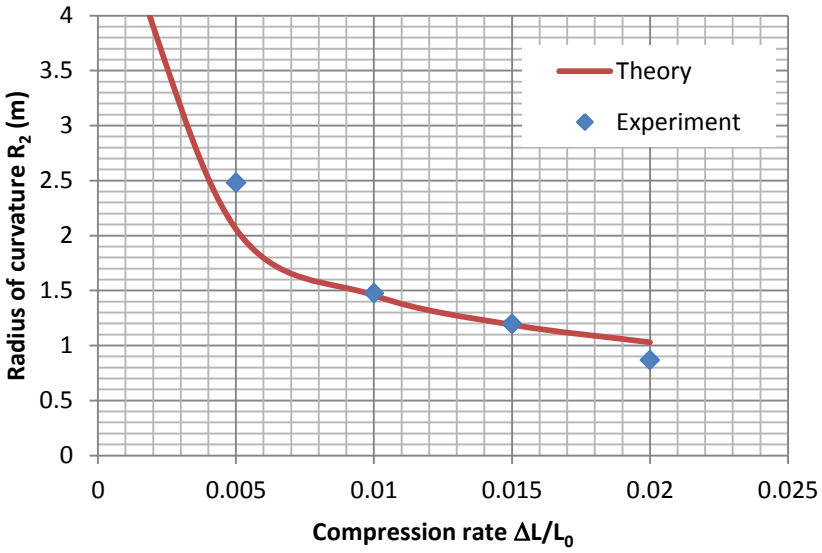

Figure 13 - Longitudinal curvature of spine

7. Conclusions

The analysis described above should be regarded as first approximation in order to maintain the simplicity of the theory. The materials are regarded as linear elastic, the bending analysis for the diaphragm in Section 4 is based on small deflection assumption in order to keep the material selection index simple and the linear relationship of force vs displacement is applied in Section 5 for simplicity. These simplifying assumptions may be responsible for the discrepancy observed in the comparison with experimental measurements in Figure 11 – Figure 13. Nevertheless, the theory of spine control predicts the trends of the diaphragm deflection and the radius of curvature of spine correctly. Therefore the theory can be used as a quick tool to predict the behaviour of the structure of other scale models of different material combinations. To predict the behaviour of the structure more accurately will require a full 3D FEA model to account for the realistic boundary conditions and the extension of the edge strings. Nevertheless, these conclusions can be drawn:

(1) The design constraints for the diaphragm of a wave energy converter were identified including the bending strain, the buckling limit due to in-plane compression and the corrosive marine environment.
(2) A formula for the transverse buckling load of the diaphragm was derived as a function of material properties. An index for material selection was formulated. The best candidates were identified using CES and discussed regarding the design constraints.
(3) A simplified theory was derived using minimum potential energy principle to predict the shape of the diaphragm at varying spine compression.

Measurements of spine and diaphragm displacements were carried out under various spine compressions. The results of diaphragm deflection and radius of curvature of spine are in good agreement with theoretical predictions. Some stiffening of the diaphragm with increasing deflection was also noted.

Acknowledgements

Thanks to Sea Energy Associates Ltd. for the use of the physical model for analysis and measurement. Plymouth University is acknowledged for funding this study. The building of the new 1/5th scale physical model was supported by a Santander Seedcorn Scholarship for KMC. The authors are grateful for the support of engineering technician team (Greg Nash, Terry Richardson).

References

1. Wave and tidal energy in the UK 2013: Conquering challenges, generating growth. London: RenewableUK; 2013.

2. Accelerating marine energy. Carbon Trust; 2011.
3. Marine energy in the UK: State of the industry report 2012. RenewableUK; 2012.
4. 2050 Pathways Analysis. Department of Energy and Climate Change, UK; 2010.
5. UK Renewable energy roadmap. Department of Energy and Climate Change, UK; 2011.
6. Global technology review. Devon, UK: Marine Energy Matters; 2014.
7. Wave Energy Technology Brief. International Renewable Energy Agency, 2014.
8. A valuation of the UK's offshore renewable energy resource. The Offshore Valuation Group, Public Interest Research Centre; 2010 ISBN 978-0-9503648-8-9.
9. Bruckner T, Bashmakov IA, Mulugetta Y, et al. Energy Systems. In: Edenhofer OR, Pichs-Madruga Y, Sokona E, et al, editors. Climate Change 2014: Mitigation of Climate Change: Cambridge University Press, UK; 2014.
10. Leijon M, Danielsson O, Eriksson M, Thorburn K, Bernhoff H, Isberg J, et al. An electrical approach to wave energy conversion. Renewable Energy. 2006;31(9):1309-19.
11. Drew B, Plummer AR, Sahinkaya MN. A review of wave energy converter technology. Proceedings of the Institution of Mechanical Engineers, Part A: Journal of Power and Energy. 2009;223(8):887-902.
12. Wave Devices: European Marine Energy Centre; 2014 [30/03/2015]. Available from: http://www.emec.org.uk/marine-energy/wave-devices/.
13. Babarit A, Hals J, Muliawan MJ, Kurniawan A, Moan T, Krokstad J. Numerical benchmarking study of a selection of wave energy converters. Renewable Energy. 2012;41(0):44-63.
14. Oyster 1, Orkney: Aquamarine Power; [26/03/2015]. Available from: http://www.aquamarinepower.com/projects/oyster-1-orkney/.
15. de Andres A, MacGillivray A, Guanche R, Jeffrey H. Factors affecting LCOE of Ocean energy technologies: a study of technology and deployment attractiveness. 5th International Conference on Ocean Energy; Halifax, Nova Scotia2014.
16. Bellamy NW. The Circular Sea Clam Wave Energy Converter. In: Evans DV et al, editor. Hydrodynamics of Ocen Wave-Energy Utilization: Springer-Verlag Berlin; 1986. p. 69-79.
17. Farley FJM, inventor; Farley, F. J. M., assignee. Free floating bellows wave energy converter. Intellectual Property Office, UK 21 February 2011.
18. Lu K. Materials in Energy Conversion, Harvesting, and Storage: John Wiley & Sons, Inc.; 2014. 448 p.
19. Ashby F. Materials and the Environment: Eco-informed Material Choice: Butterworth-Heinemann; 2013.
20. Bellamy NW, Bellamy NM, Smith RI. Energy converter. Google Patents; 2012.
21. van Nieuwkoop JCC, Smith HCM, Smith GH, Johanning L. Wave resource assessment along the Cornish coast (UK) from a 23-year hindcast dataset validated against buoy measurements. Renewable Energy. 2013;58(0):1-14.
22. Shigley J, Mischke C, Budynas RG. Mechanical Engineering Design: McGraw-Hill Higher Education; 2003.
23. Ashby MF. Materials Selection in Mechanical Design. 3rd ed: Butterworth-Heinemann; 2005.
24. Thakker A, Jarvis J, Buggy M, Sahed A. A novel approach to materials selection strategy case study: Wave energy extraction impulse turbine blade. Mater Design. 2008;29(10):1973-80.
25. Summerscales J, Short D. Carbon fibre and glass fibre hybrid reinforced plastics. Composites. 1978;9(3):157-66.
26. Mouritz AP, Gellert E, Burchill P, Challis K. Review of advanced composite structures for naval ships and submarines. Composite Structures. 2001;53(1):21-42.
27. Garcia-Espinel JD, Castro-Fresno D, Gayo PP, Ballester-Munoz F. Effects of sea water environment on glass fiber reinforced plastic materials used for marine civil engineering constructions. Mater Design. 2015;66:46-50.

28. Jacob A. Wave power converter relies on composites 2009. Available from: http://www.materialstoday.com/composite-applications/news/wave-power-converter-relies-on-composites/.
29. Fatigue in Composites. Harris B, editor. Cambridge: Woodhead Publishing; 2003.
30. Ghali A, Neville A. Structural Analysis: A unified classical and matrix approach. 3rd ed. London: E & FN Spon Press; 1989.
31. Plastics International. Materials Properties [30/03/2015]. Available from: http://www.plasticsintl.com/.